nature structural & molecular biology

Signaling conformations of the tall cytokine receptor gp130 when in complex with IL-6 and IL-6 receptor

Georgios Skiniotis[1], Martin J Boulanger[2], K Christopher Garcia[2] & Thomas Walz[1]

gp130 is a shared cytokine signaling receptor and the founding member of the 'tall' class of cytokine receptors. A crystal structure of the ligand-binding domains of gp130 in complex with human interleukin-6 (IL-6) and its α-receptor (IL-6Rα) revealed a hexameric architecture in which the gp130 membrane-distal regions were ~100 Å apart, in contrast to the close apposition seen between short cytokine receptor complexes. Here we used single-particle EM to visualize the entire extracellular hexameric IL-6–IL-6Rα–gp130 complex, containing all six gp130 domains. The structure reveals that gp130 is bent such that the membrane-proximal domains of gp130 are close together at the cell surface, enabling activation of intracellular signaling. Variation in the receptor bend angles suggests a possible conformational transition from open to closed states upon ligand binding; this transition is probably representative of the other tall cytokine receptors.

Ligand-mediated clustering of receptor extracellular domains into precise geometric architectures is necessary to elicit intracellular signaling cascades. One example is gp130, which is a shared signal transducing receptor for a family of four-helix bundle cytokines including IL-6, viral IL-6, leukemia inhibitory factor (LIF), ciliary neurotrophic factor (CNTF), oncostatin M (OSM), interleukin-11 (IL-11) and cardiotrophin 1 (CT-1)[1]. gp130 is the founding member of a group of tall cytokine receptors that includes LIF-R, OSM-R, G-CSF-R and others, characterized by the presence of three membrane-proximal fibronectin-III (FNIII) domains[2]. gp130 signaling is critical to the normal growth and differentiation of numerous tissue types, and derangements in gp130 signaling have been implicated in many diseases and neoplastic disorders. gp130 engagement leads to activation of src and JAK/Tyk tyrosine kinases, as well as the STAT family of transcription factors[3]. The prototypic gp130-cytokine is IL-6, which is a primary mediator of hematopoietic cell growth and differentiation, as well as a proinflammatory cytokine that plays a central role in host defense against infection and tissue injuries[4].

Cytokines that activate gp130 share a common, classical four-helix-bundle fold[5]. Extensive structure-function studies have revealed that gp130 engagement occurs through three conserved receptor-binding epitopes on the cytokines, the third of which is unique to gp130 cytokines[2]. The gp130 extracellular domain is composed of six β-sheet sandwich domains. Cytokine engagement by gp130 occurs through the three membrane-distal domains (D1–D3)[6,7], whereas the three membrane-proximal FNIII domains (D4–D6) do not play a specific role in recognition, but are required for receptor activation[4] (**Fig. 1a**). The three membrane-proximal FNIII domains are a conserved feature of all members of the tall receptors that raise the ligand-binding sections of the receptors a substantial height off of the cell surface[8]. Activation of gp130 by IL-6 has been shown to proceed in a sequential fashion whereby IL-6 first engages IL-6Rα through a 'site I' interaction. This binary complex (IL-6–IL-6Rα) is then competent to engage the gp130 cytokine-binding homology region (CHR) via site II, located at gp130 D2–D3, to form an intermediate nonsignaling trimolecular complex. This trimolecular complex then dimerizes via the interaction of the cytokine site III and the gp130 D1, or Ig-like domain (IgD)[7,9].

A recent structural study has shown that the extracellular gp130 signaling complex with IL-6 assembles into a hexameric architecture containing two copies each of IL-6, IL-6Rα and gp130 (ref. 9; **Fig. 1b**). This 'hexamer' contains the top three domains of gp130, which are arranged in an antiparallel dimer with a total of ten symmetry-related receptor-ligand and receptor-receptor interfaces. This hexameric 'cap' must position the gp130 intracellular domains into a precise orientation and proximity required for transphosphorylation by the associated JAK kinases[10]. However, because the crystal structure did not contain the three membrane-proximal gp130 domains, a lingering question has been the disposition of these 'legs' as they enter the membrane. Compounding this question has been the fact that, in the hexamer structure, the gp130 D3 domains extend away from one another so that if D4–D6 projected straight outward, they would enter the membrane hundreds of angstroms away from each other (**Fig. 1b**). Given that the paradigm for cytokine receptor activation is to bring the intracellular JAKs to within close proximity[11], it has become important to resolve the question of the structure of the legs of gp130 within the hexamer. Similar to the hexameric assembly of the 'headpiece,' the disposition of the legs will probably be conserved across all members of the gp130 family of tall cytokine receptors. Previous biochemical and thermodynamic data

[1]Department of Cell Biology, Harvard Medical School, 240 Longwood Avenue, Boston, Massachusetts 02115, USA. [2]Departments of Microbiology and Immunology, Structural Biology, Stanford University School of Medicine, Stanford, California 94305, USA. Correspondence should be addressed to K.C.G. (kcgarcia@stanford.edu) or T.W. (twalz@hms.harvard.edu).

Published online 15 May 2005; doi:10.1038/nsmb941

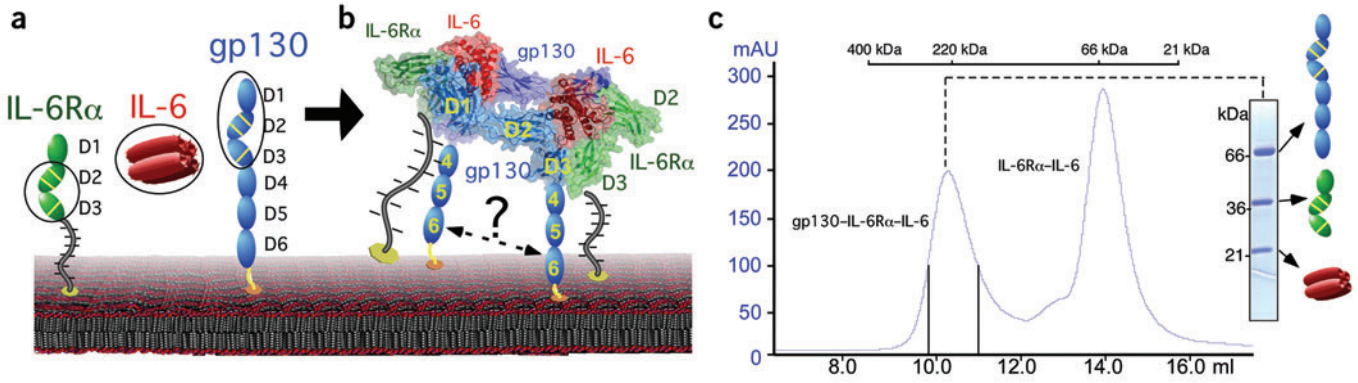

Figure 1 The components of the gp130–IL-6 system. (**a**) Schematic models of the domain structure of the IL-6Rα, IL-6 and gp130. Each domain in both receptors is a ~110-residue β-sheet sandwich domain. The top, or D1 domains, of IL-6Rα and gp130 are Ig-like domains (IgD), followed by the cytokine-binding homology region (CHR) at D2 and D3. The membrane-proximal regions of gp130 are defined as the D4–D6 FNIII domains. (**b**) The crystal structure of the gp130(D1–D3)–IL-6–IL-6Rα(D2–D3) hexameric complex[9] is shown as a transparent surface representation connected to schematic representations of the gp130 legs, roughly to scale. As indicated, the hexamer contains two copies each of gp130, IL-6 and IL-6Rα in which the gp130–IL-6–IL-6Rα trimolecular complexes are dimerized in an antiparallel orientation. The angular projection of the legs from the base of the gp130 hexamer (that is, D3) results in a large separation as the receptor enters the membrane. (**c**) Gel filtration of the hexamer containing the entire gp130 extracellular domain (D1–D6) eluting at the expected molecular mass (~250 kDa). The slower migrating peak contains excess IL-6–IL-6Rα binary complex.

support a model whereby the legs are in close contact in the signaling active complex on the cell surface[9,12].

To study the conformation of the gp130 legs in a signaling context, we used single-particle EM to visualize the entire *in vitro*–reconstituted extracellular gp130 (D1–D6) in complex with IL-6 and IL-6Rα (D1–D3). The three-dimensional structure of this signaling complex reveals that the gp130 legs bend toward one another and thus bring the D6 domains into close proximity. The EM data also reveal a diverse population of particles with different extents of leg closure, which we speculate may be snapshots of intermediate states of the receptor during a ligand-induced conformational change.

RESULTS

Expression of the IL-6–IL-6Rα–gp130 complex

Previously we expressed and determined a crystal structure of a soluble complex containing the gp130 D1–D3 domains, the D2 and D3 domains of the IL-6 α-receptor, and human IL-6 (refs. 7,9; **Fig. 1b**). For the present study we expressed a similar hexameric complex in baculovirus, except that we used the entire gp130 extracellular domain containing D1–D6, as well as all three extracellular domains of the IL-6Rα (D1–D3). Both constructs contained a C-terminal His-tag that was used for affinity purification. The complex eluted from gel filtration at the expected molecular mass of ~250 kDa for a 2:2:2 hexameric complex (**Fig. 1c**). This material was used for the subsequent EM experiments.

Projection analysis of the IL-6–IL-6Rα–gp130 complex

As a first step in the structural characterization of the IL-6–IL-6Rα–gp130 hexameric complex, we recorded images of negatively stained samples. The images showed the complexes to be monodisperse and similar in size, but the particles exhibited different shapes (**Fig. 2a**). To analyze the structural heterogeneity in the particle population we interactively selected ~21,000 particles from 130 digitized images and classified them into 100 classes. The class averages (representative averages are shown in **Fig. 2b**) revealed that the complexes adsorbed to the carbon support film in only two preferred orientations. The majority of the class averages (comprising >90% of all the particles) showed the complex to have a roughly triangular shape (**Fig. 2b**, panels 1–9), whereas the remaining class averages (comprising <10% of the particles) showed particles with a rectangular shape (**Fig. 2b**, panel 10). These two types of particles could already be clearly distinguished in the raw images (red and black arrows in **Fig. 2a** indicate rectangular and triangular particles, respectively).

All the class averages representing the rectangular particles revealed very similar features and showed a two-fold symmetric molecule with a distinct accumulation of stain in the center, representing a hole or cavity at this position (**Fig. 2b**, panel 10). Comparison with the recently determined crystal structure of the hexameric complex lacking the membrane-proximal domains[9] revealed that the rectangular particles represent top (or bottom) views of the complex (**Fig. 2c**,**d**). The averages of the top-view particles did not show a density for the D1 domain of IL-6Rα, which is present in the construct used for this EM study but was missing in the construct used to solve the crystal structure[9]. The IL-6Rα D1 domain is not involved in ligand binding. The interface between the IL-6Rα D1 and D2 domains is small and probably a flexible hinge, allowing the D1 domain to project outward from the body of the complex in many different orientations, causing it to disappear upon averaging.

In contrast to the rectangular top views, the triangular side views of the IL-6–receptor complex revealed substantial variability (**Fig. 2b**, panels 1–9). The head domains of the particles (top part in the projections) seem to have a consistent shape and can easily be interpreted in terms of the crystal structure of the hexameric complex (**Fig. 2e**,**f**). By contrast, the legs of the particles representing the D4–D6 domains of the two gp130 molecules (bottom part in the projections) appear quite different in individual class averages and thus seem to be the main source for the structural heterogeneity in the imaged complexes.

None of the averages representing the side view particles exhibited a clear two-fold symmetry, mostly because one of the legs always seemed to be more bent than the other. In almost all the averages that showed densities for the entire legs, the legs interacted with each other. In most cases the interaction was confined to the very tips of the legs (for example, **Fig. 2b**, panels 1–3), suggesting that the D6 domain is most important for the interaction between the membrane-proximal leg regions. In a smaller number of averages the legs seemed to be less extended and to interact over a longer stretch. In these complexes the interactions between the two legs may thus also involve the D5 domains of gp130 (for example, **Fig. 2b**, panels 5–7).

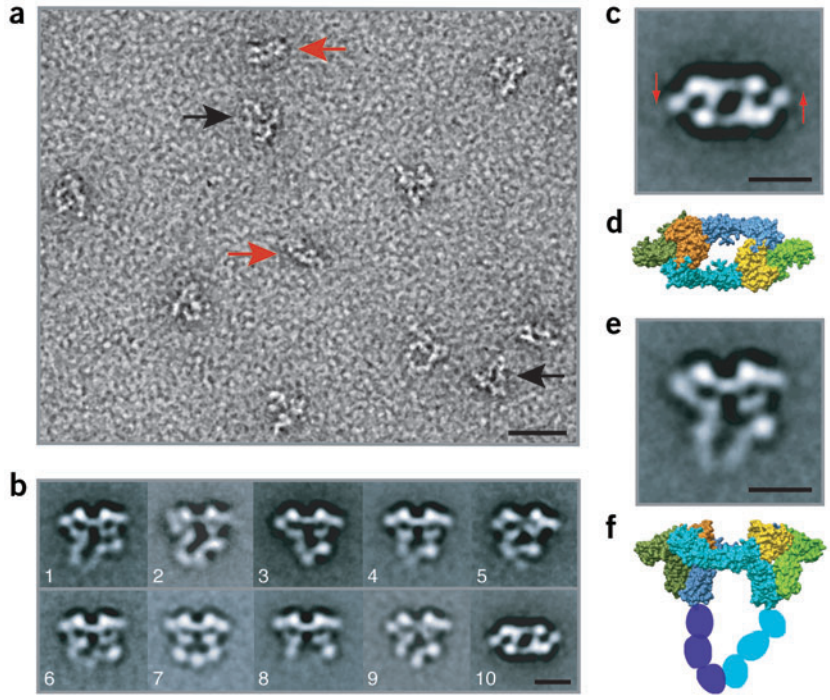

Figure 2 EM of the IL-6–IL-6Rα–gp130 complex. (**a**) Raw image of negatively stained complexes showing rectangular top views (red arrows) and triangular side views (black arrows). (**b**) Representative class averages resulting from the image classification. (**c**,**d**) Class average of top-view particles and the corresponding view on the crystal structure of the hexameric IL-6–IL-6Rα–gp130 complex[9]. Red arrows in **c** indicate the expected positions of the D1 domains of IL-6Rα. (**e**,**f**) Selected class average of side-view particles and the corresponding view on the crystal structure. The ovals in **f** represent the gp130 D4–D6 domains missing in the crystal structure. Scale bar in **a**, 25 nm. Scale bars in **b**, **c** and **e**, 10 nm.

None of the averages in which the two legs were clearly resolved showed the legs to be completely separated. However, in many averages the lower part of one or even both legs was not represented by clear densities (for example, **Fig. 2b**, panels 8 and 9). This could reflect increased flexibility of the lower legs as soluble molecules when released from the constraints of the cell surface, causing the lower legs to be averaged out. We do not believe this to be the case, because the raw images showed that the overwhelming majority of particles adopted a closed leg conformation, showing that the membrane-proximal regions of the gp130 legs have a strong tendency to interact. Notably though, the legs do not appear as rigid rods, but acquire different bent angles at the FNIII transitions, resulting in different extents of closure. This heterogeneity in the degree of leg closure suggests the possibility of a conformational transition upon ligand binding from an open to closed state (discussed below).

Structure of the IL-6–IL-6Rα–gp130 complex

For a more complete understanding of the conformation of the gp130 legs, we calculated a three-dimensional reconstruction of the IL-6–receptor complex. We recorded 83 pairs of images at tilt angles of 60° and 0°, from which we interactively selected ~18,000 particle pairs. The particles from the images of the untilted specimen were classified into 78 classes (see **Supplementary Fig. 1** online). Because the increased flexibility in the gp130 legs would limit the definition of our three-dimensional map, we chose only three of the most similar class averages representing the predominant conformation of the complex (with the legs interacting via their tips) and exhibiting the most distinct fine structure for the entire length of the leg (marked in red in **Supplementary Fig. 1**). In the final three-dimensional reconstruction we also included the images from the untilted specimen in three of the classes representing the top-view particles (marked in yellow in **Supplementary Fig. 1**).

The three-dimensional reconstruction of the hexameric assembly at a resolution of ~35 Å (as judged by Fourier shell correlation (FSC), see **Supplementary Fig. 2** online) reveals the triangular shape of the side view (**Fig. 3a**) and the rectangular shape of the top view of the complex (**Fig. 3b**) already seen in the raw images (**Fig. 2a**) and projection averages (**Fig. 2b**). The density map has dimensions of 17.5 × 15.5 × 7 nm (width × height × depth). It nicely resolves the elongated bipartite head domain that corresponds to the ectodomain complex of IL-6 and the cytokine-binding regions of IL-6Rα and gp130, and the two legs that represent the membrane-proximal D4–D6 domains of gp130. The two legs have quite distinct appearances. Whereas one leg is represented by a straight density of approximately constant diameter (**Fig. 3d**), the other leg is represented by a kinked density of uneven diameter (**Fig. 3c**). Although we cannot exclude that the two legs indeed assume different conformations *in situ*, we believe that the differences between the two legs seen in the three-dimensional reconstruction are preparation artifacts. We interpret the straight leg to be in contact with the carbon film and to be therefore represented rather accurately in the density map. By contrast, the kinked leg is connected to the head domain at a distance from the carbon support. It thus starts at an elevated position, and (at the point marked by an arrow in **Fig. 3a**,**c**) collapses onto the carbon film upon dehydration of the specimen. We believe that this is the reason for the kink observed in the density for this leg. Because one leg appears to collapse in more or less the same fashion in all the imaged particles, this suggests that the linker between the D3 and D4 domains of gp130 is most flexible and may constitute a hinge between the head and leg domain in this molecule.

Molecular modeling of the IL-6–IL-6Rα–gp130 complex

To assess the quality of our three-dimensional reconstruction and gain further insight into the interacting modules between the membrane-proximal gp130 domains, we manually fit the available crystal structures into our density map. Owing to the limited resolution of the map we made no attempt to use computational algorithms to optimize the fit of the crystal structures into the density. The crystal structure of the hexameric ectodomain of the gp130–receptor complex[9] fit almost perfectly into the corresponding portion of the density map (**Fig. 3a**,**b**). Consistent with the projection averages, the three-dimensional map also lacks any density for the D1 domains of IL-6Rα, which is probably due to flexibility of the linker connecting the D1 domain to the rest of the complex. The position for the D1 domain shown in **Figure 3** is thus based on the crystal structure of the unliganded IL-6Rα domains D1–D3 (ref. 13). To model the D4–D6 domains of gp130 we used the fibronectin FNIII domains 7–9, which we extracted from the crystal structure of the human fibronectin 7–10 fragment[14]. The structures for fibronectin domains 7–9 were individually fit into the density map to approximate

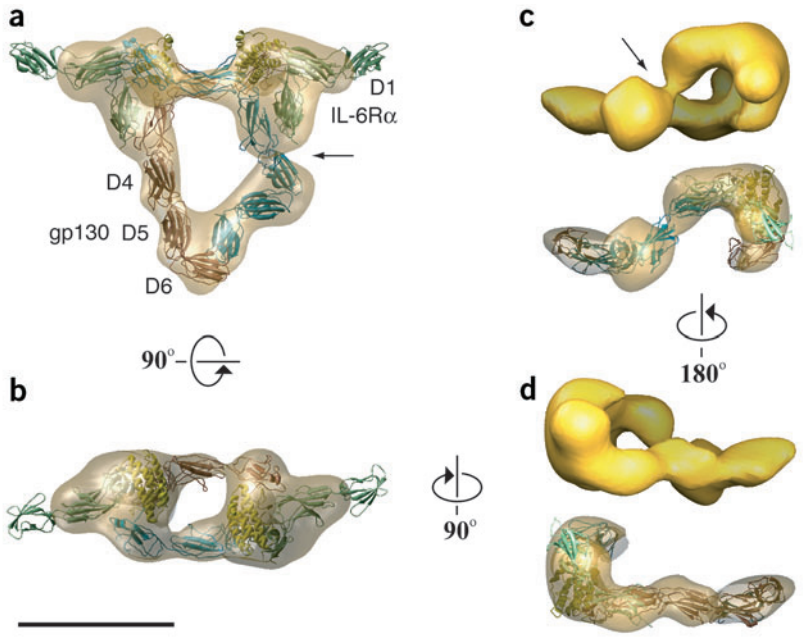

Figure 3 Three-dimensional map and fit crystal structures of the IL-6–IL-6Rα–gp130 complex. (**a**,**b**) Side and top view on the hexameric complex revealing the good fit of the crystal structure of the gp130(D1–D3)–IL-6–IL-6Rα(D2–D3) complex[9] into the EM density map. Density for the D1 domain of IL-6Rα is missing in the EM map, presumably owing to the flexibility of the linker between the D1 and D2 domains. (**c**,**d**) View of the gp130 legs with the fit FNIII domains used to model gp130 domains D4–D6. Top panels, EM density map for the entire complex. In the bottom panels, the gp130 leg in the back was removed to allow for a better view of the docking of the crystal structures into the front leg. Arrows in **a** and **c** indicate the position where the 'kinked' leg collapsed onto the carbon film. Scale bar, 10 nm.

the structure for the two legs (**Fig. 3a**,**c**,**d**). The fit is quite good apart from the region that corresponds to the D4 domain of the kinked leg, where the electron density is larger, probably as a result of the collapse of this leg onto the carbon film (discussed above). Our density map lacks the resolution to propose atomic-resolution interactions between the legs. However, our model argues that in the predominant conformation of the IL-6–receptor complex, the two D5 domains do not contribute to the interaction between the two gp130 legs. It is thus mainly the two D6 domains that homodimerize and cause the closure of the legs with the resulting spatial proximity of the transmembrane and cytoplasmic domains of the two gp130 molecules in the signaling complex.

DISCUSSION

gp130 is the prototypic member of the tall class of cytokine receptors that includes LIF-R, OSM-R, IL-12-R, G-CSF-R and several others. This family of receptors has two unique features relating to cytokine recognition and activation compared with members of the short cytokine receptor family such as the human growth hormone receptor[2,7–9] (**Fig. 4a**,**b**). The first is the presence of a top-mounted IgD that is necessary for receptor activation. Resolution of crystal structures of D1–D3 fragments of gp130 with human and viral IL-6 clarified the role of this domain in forming a direct interaction with a 'site III' on the cytokine that serves to dimerize gp130 (refs. 7,9).

The second defining feature of the tall class of cytokine receptors is the presence of the three membrane-proximal FNIII domains supporting the membrane-distal ligand-binding regions. In the crystal structures of the viral and human gp130 complexes, the bases of the gp130 D3 domains are ~180 Å apart, and are angled away from the center of the complex (**Fig. 1b**). If the D4–D6 domains project straight outward, as is seen in several FNIII-containing structures, such as fibronectin, then the membrane-proximal regions would enter the membrane ~300 Å apart. The accepted paradigm for activation of the short class of cytokine receptors is that the ligand serves to bring the receptors together in close proximity[15], as was originally shown in the human growth hormone system[11,16] (**Fig. 4a**). In that complex, which is generally representative of other short cytokine receptor complexes (containing two receptor extracellular domains) such as those formed with prolactin, erythropoietin, interferon and others, the base of the receptors are in direct contact[17–20]. This contact would translate into a close apposition of the intracellular signal transduction components such as the JAKs, which are bound to cytokine receptor intracellular regions. When brought within close proximity and in the correct orientation, the JAKs will phosphorylate one another, instigating a downstream signaling cascade[10]. Therefore, the notably large separation of the gp130 D1–D3 extracellular complexes, and the disposition of the membrane-proximal regions, has been an important issue to resolve.

The EM structure of the full hexameric complex is notable in two respects. First, it confirms the architecture of the hexameric membrane-distal ligand-binding complex whose crystal structure has been determined[9]. This architecture rationalizes the engagement of the three sites, I–III, found on all tall receptor cytokines. However, different theoretical models have persisted based on the suggestion that the legs may substantially alter the hexameric structure[13,21]. Clearly this is not the case as the ring-like hexameric architecture of the ternary complex is well resolved in the EM maps (**Figs. 2c**,**d** and **3b**). This basic topological blueprint for the simultaneous receptor engagement of three cytokine epitopes serves as a template for the assembly and structures for all tall cytokine receptor complexes. The tall receptor cytokines (such as OSM, LIF, IL-6, IL-11, CNTF, IL-12, leptin and G-CSF) all contain the site III epitope that distinguishes them from the short receptor cytokines (such as hGH, EPO and IFN), which only contain sites I and II (**Fig. 4a**,**b**).

The second issue the EM structure resolves is the disposition of the gp130 legs. It is apparent that the legs are in close proximity in the hexameric signaling complex. The close proximity of the most membrane-proximal receptor domains is similar to that seen in the short cytokine receptor complexes such as hGH[16]. This is achieved by bending of the gp130 legs at apparent flexible hinges between the D3-D4 and D4-D5 boundaries. There is previous biochemical evidence for interaction between the gp130 legs. In one study, a cytokine-induced disulfide bonded dimer is formed between the gp130 D5 domains upon introduction of a cysteine mutation in D5 (ref. 12). In another study, a comparison of the entropies of complex formation between a legless construct (D1–D3) and one with legs revealed that the legless hexamer had a more favorable entropy[9]. That is, the presence of the legs resulted in a rigidification of the system upon IL-6 binding, suggesting an interaction between the legs that reduces conformational flexibility. We interpreted these data to mean that in the absence of ligand, the legs have some degree of flexibility, which is then rigidified upon formation of the hexamer through direct leg-leg contact.

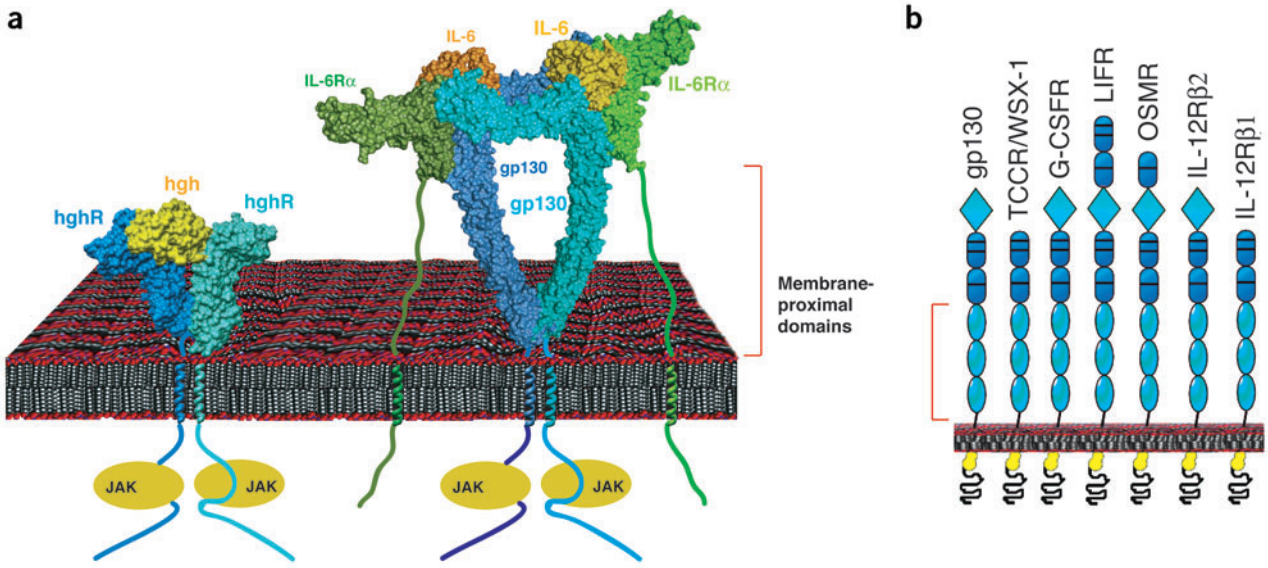

Figure 4 Structural comparison of short and tall cytokine receptor complexes. (**a**) The structure at left is the 1:2 human growth hormone (hGH)–receptor complex in which the receptor is composed of a single CHR (two β-sheet sandwich domains)[16]. At right is our model of the gp130 hexamer including the membrane-proximal legs, which elevate the ligand-binding regions (membrane-distal) substantially off the cell surface. The bending of the legs allows gp130 to form receptor-receptor contact before entering the cell membrane, enforcing a close apposition of the receptor dimer and instigating JAK transphosphorylation in the intracellular domains. The height of the IL-6Rα off of the membrane, connected by a peptide region, is not known but only approximated for this figure. (**b**) The family of tall receptors containing three membrane-proximal FNIII domains. We propose that similar bent leg conformations exist in signaling complexes containing these receptors.

The projection averages of the negatively stained particles reveal substantial heterogeneity in the exact position of the legs, with different classes that are in different states of closure (**Fig. 2b**). It is possible that these different classes reflect 'metastates' in a transition between an open unliganded gp130 and a closed liganded gp130 in the hexameric complex. Such intermediates were also observed in EM structures of integrins, which contain markedly similar legs to gp130 that appear to change their orientation during receptor activation[22]. In this respect, one needs to consider the spatial constraints of gp130 on the membrane (**Fig. 4a**). The IL-6 α–receptor is connected to the membrane by a 40-residue stalk region that, if fully extended, would be ~110 Å. This distance would raise the CHR region off the cell surface the distance of approximately three FNIII domains. The gp130 CHR (D2–D3) is raised off the cell surface by three FNIII domains, but gp130 also has a connecting peptide linking the D6 domain to the cell surface, raising it higher off the membrane. Therefore, the IL-6Rα CHR would sit lower than the gp130 CHR, possibly requiring a lowering of gp130 in order to form a trimolecular IL-6–IL-6Rα–gp130 complex. This lowering mechanism seems to be the bending of the legs to compensate for the 'lower' height of the IL-6 complex. In this fashion, we suggest that the discordance in the height of the IL-6Rα and gp130 ligand-binding regions induces bending of gp130 upon IL-6 engagement, which simultaneously brings the bases of the gp130 monomers together to activate signaling. Therefore, the ligand-induced adjustment of the height of gp130-binding domains may have the indirect result of closing the gap between the legs through a 'squatting' type of mechanism. However, in cases in which gp130 does not pair with a shorter α receptor, such a squatting mechanism would not be required. In these cases, such as would be used by G-CSF, leptin-R and others, if the unliganded tall receptors exist as a dimer on the cell surface, as has been proposed[23], a simple conformational transition involving reorientation of the legs through a flexible hinge may be necessary to convert the receptor from a quiescent to active state. Ultimately, definitive proof of a conformational switch from open to closed legs will require structural analysis of unliganded gp130. However, regardless of whether the transition involves a 'height adjustment' or simple gp130 dimer reorientation, we believe our data strongly indicate a bending of the receptor, induced by ligand binding, in synchrony with receptor activation.

The tall class of cytokine receptors uses a common assembly template, based on the hexamer structure, for the ligand-binding regions (**Fig. 4b**). Therefore they share the problem of how to close the large gap between the legs as the receptors enter the cell membrane. We propose that other members of this receptor family, which contain the characteristic FNIII membrane-proximal domains, use a similar bent conformation of the legs to minimize the receptor-receptor distance in the signaling dimer.

METHODS

Protein expression and purification. The extracellular domains of human gp130 (D1–D6, residues 1–610), IL-6Rα (D1–D3, residues 1–310) and human IL-6 were subcloned by PCR into the baculovirus expression vector pAcgp67A. For production of the hexameric complex, recombinant viruses for IL-6 and IL-6Rα were used to coinfect Hi5 insect cells, and gp130 was expressed alone. The IL-6–IL-6Rα complex and gp130 were purified separately from the insect cell supernatant using Ni-agarose and gel filtration chromatography. As quantities of gp130 were limiting, the three components were mixed with an excess of the IL-6–IL-6Rα binary complex. This mixture was separated by gel filtration FPLC, which showed two peaks. The faster eluting peak contained the IL-6–IL-6Rα–gp130 complex and the second peak contained the excess IL-6–IL-6Rα complex. The IL-6–IL-6Rα–gp130 complex eluted at the expected position (~250 kDa) for a hexameric complex containing two copies of each component. This material, in HEPES-buffered saline, pH 7.2, was subsequently used for the EM studies.

Electron microscopy. IL-6–IL-6R–gp130 complexes were prepared for EM using the conventional negative staining protocol[24]. Briefly, 3 μl of sample was adsorbed to a glow-discharged carbon-coated copper grid, washed with two drops of deionized water, and stained with two drops of 0.75% (w/v) uranyl formate. The sample

was imaged at room temperature with a Tecnai T12 electron microscope equipped with an LaB_6 filament and operated at an acceleration voltage of 120 kV. Images of specimens tilted to 60° and 0° were recorded using low-dose procedures at a magnification of 52,000× and a defocus value of about –1.5 μm. Images were taken on Kodak SO-163 film and developed for 10 min with full-strength Kodak D-19 developer at 20 °C.

Two-dimensional image processing and three-dimensional reconstruction. Micrographs were digitized with a Zeiss SCAI scanner using a step size of 7 μm, and 3 × 3 pixels were averaged to obtain a pixel size of 4.04 Å on the specimen level. For the projection analysis 21,073 particles were interactively selected from 130 images using WEB (associated with the SPIDER suite[25]). The particles were windowed into 100 × 100 pixel images and subjected to ten cycles of multireference alignment and classification specifying 100 output classes. Representative class averages are shown in **Figure 2b**.

Our projection analysis revealed substantial structural heterogeneity, which makes the IL-6–receptor complex unsuitable for vitrification and structure determination by cryo-EM. Furthermore, because negative staining caused the complex to adsorb to the carbon film in only two orientations, the random conical tilt technique, implemented in SPIDER[25], was the only option to produce a three-dimensional density map. We interactively selected 17,826 pairs of particles from 83 micrograph pairs taken at tilt angles of 60° and 0°, and windowed them into 100 × 100 pixel images. The particles from the images of the untilted specimen were subjected to ten cycles of multireference alignment and classification specifying 78 output classes (see **Supplementary Fig. 1**). The particle images from three classes that produced very similar projection averages (marked in red in **Supplementary Fig. 1**) were combined and used for three-dimensional reconstruction with the random conical tilt technique[26]. Because the combined classes contained only 783 out of the ~18,000 particle pairs, we attempted to include more particles from similar classes. This caused, however, a reduction in the quality of the final three-dimensional reconstructions and was therefore not further pursued. A first back-projection map was calculated using only the 783 particles from the images of the tilted specimen. After angular refinement, the corresponding particles from the images of the untilted specimen were added and the images were subjected to another cycle of angular refinement. Further refinement of the orientational parameters as well as contrast transfer function correction was carried out using FREALIGN[27].

The resulting density map showed all the features seen in the class averages but much less structural detail in the direction perpendicular to the carbon film (*z*-direction), which was particularly evident in the head region (see **Supplementary Fig. 3** online). The lack of features in the *z*-direction was most likely due to a combined effect of the missing cone problem and specimen collapse. The missing cone problem reflects the technical limitation that a specimen can be tilted only to ~60° in the electron microscope, leaving a cone-shaped region in Fourier space that cannot be sampled. Because of this cone-shaped region of missing data, the resolution in *z*-direction is lower than the in-plane resolution. The bigger problem was, however, specimen collapse, which results from the dehydration of the specimen and is unavoidable with the conventional negative staining protocol used in this study. To improve structural detail in the *z*-direction we included 630 top view-particles from the images of the untilted specimen that produced the class averages marked in yellow in **Supplementary Figure 1**. Alignment of these particle images to the density map shown in **Supplementary Figure 3** using FREALIGN[27] did not result in a visible improvement of the features in the *z*-direction, indicating that the top-view images did not align correctly to the model (the angles assigned to the images in this step are shown in the angular distribution plot in **Supplementary Fig. 2**).

To obtain a better model for the alignment of the top-view images, we fit the available crystal structures into the density map. The head domain of the IL-6–receptor complex was fit with the corresponding crystal structure of the hexameric complex (PDB entry 1P9M[9]), whereas the D4–D6 domains of gp130 were modeled using fibronectin FNIII domains 7–9 (PDB entry 1FNF[14]). We then calculated a density map from the pseudo-atomic model and filtered it to a resolution of 30 Å. The side view of the resulting density map was very similar to the initial three-dimensional reconstruction, but the top view showed significantly more fine structure compared to the initial experimental map (compare right and left panels in **Supplementary Fig. 3**). This improved density map was then used as reference model to determine the correct orientational parameters for the 630 top view particles (see **Supplementary Fig. 2b**).

The final density map after five refinement cycles of all the particle images with FREALIGN[27] is shown in **Figure 3** and **Supplementary Figure 3**. The angular distribution for all the 2,196 particles used in the final reconstruction is shown in **Supplementary Figure 2**. The resolution of the final reconstruction was assessed by FSC, which suggests a resolution of 32 Å with the FSC = 0.15 criterion[28] or a resolution of 37 Å with the more conservative FSC = 0.5 criterion (see **Supplementary Fig. 2**).

Fit of crystal structures into the EM density map. The crystal structures were visually fit into the EM density map using O[29]. Owing to the limited resolution of the density map, no attempt was made to computationally refine the fit. The atomic models used were the crystal structure of the hexameric IL-6–receptor complex (PDB entry 1P9M[9]) to model the head domain, the crystal structure of IL-6Rα domains D1–D3 (PDB entry 1N26; ref. 13) to model the IL-6Rα D1 domain, and fibronectin FNIII domains 7–9 (PDB entry 1FNF[14]) to represent gp130 domains D4–D6.

Accession codes. BIND identifers (http://bind.ca/): 262686, 262687, 262688, 262689.

Note: Supplementary information is available on the Nature Structural & Molecular Biology website.

ACKNOWLEDGMENTS

We acknowledge D. Chow, N. Goriatcheva, M. Martick and L. Brevnova for assistance and helpful discussions, and Y. Cheng for support in data collection and image processing. We also acknowledge the Keck Foundation (K.C.G.), Pew Trust (K.C.G.) and US National Institutes of Health (NIH) AI51321 (K.C.G.) for support. The molecular EM facility at Harvard Medical School was established by a generous donation from the Giovanni Armenise Harvard Center for Structural Biology and is maintained by funds from NIH GM62580 (T.W.). G.S. is a Damon Runyon Fellow, supported by the Damon Runyon Cancer Research Foundation (DRG-#1824-04).

COMPETING INTERESTS STATEMENT

The authors declare that they have no competing financial interests.

Received 18 March; Accepted 19 April 2005
Published online at http://www.nature.com/nsmb/

1. Kishimoto, T., Akira, S., Narazaki, M. & Taga, T. Interleukin-6 family of cytokines and gp130. *Blood* **86**, 1243–1254 (1995).
2. Bravo, J. & Heath, J.K. Receptor recognition by gp130 cytokines. *EMBO J.* **19**, 2399–2411 (2000).
3. Kishimoto, T., Taga, T. & Akira, S. Cytokine signal transduction. *Cell* **76**, 253–262 (1994).
4. Heinrich, P.C. *et al.* Principles of interleukin (IL)-6-type cytokine signalling and its regulation. *Biochem. J.* **374**, 1–20 (2003).
5. Bazan, J.F. Haemopoietic receptors and helical cytokines. *Immunol. Today* **11**, 350–354 (1990).
6. Bravo, J., Staunton, D., Heath, J.K. & Jones, E.Y. Crystal structure of a cytokine-binding region of gp130. *EMBO J.* **17**, 1665–1674 (1998).
7. Chow, D., He, X., Snow, A.L., Rose-John, S. & Garcia, K.C. Structure of an extracellular gp130 cytokine receptor signaling complex. *Science* **291**, 2150–2155 (2001).
8. Boulanger, M.J. & Garcia, K.C. Shared cytokine signaling receptors: structural insights from the gp130 system. *Adv. Protein Chem.* **68**, 107–146 (2004).
9. Boulanger, M.J., Chow, D.C., Brevnova, E.E. & Garcia, K.C. Hexameric structure and assembly of the interleukin-6/IL-6 α-receptor/gp130 complex. *Science* **300**, 2101–2104 (2003).
10. Ihle, J.N. Cytokine receptor signalling. *Nature* **377**, 591–594 (1995).
11. Wells, J.A. & de Vos, A.M. Hematopoietic receptor complexes. *Annu. Rev. Biochem.* **65**, 609–634 (1996).
12. Kurth, I. *et al.* Importance of the membrane-proximal extracellular domains for activation of the signal transducer glycoprotein 130. *J. Immunol.* **164**, 273–282 (2000).
13. Varghese, J.N. *et al.* Structure of the extracellular domains of the human interleukin-6 receptor α-chain. *Proc. Natl. Acad. Sci. USA* **99**, 15959–15964 (2002).
14. Leahy, D.J., Erickson, H.P., Aukhil, I., Joshi, P. & Hendrickson, W.A. Crystallization of a fragment of human fibronectin: introduction of methionine by site-directed mutagenesis to allow phasing via selenomethionine. *Proteins* **19**, 48–54 (1994).
15. Kossiakoff, A.A. & De Vos, A.M. Structural basis for cytokine hormone-receptor recognition and receptor activation. *Adv. Protein Chem.* **52**, 67–108 (1998).

16. de Vos, A.M., Ultsch, M. & Kossiakoff, A.A. Human growth hormone and extracellular domain of its receptor: crystal structure of the complex. *Science* **255**, 306–312 (1992).
17. Walter, M.R. *et al.* Crystal structure of a complex between interferon-gamma and its soluble high-affinity receptor. *Nature* **376**, 230–235 (1995).
18. Somers, W., Ultsch, M., De Vos, A.M. & Kossiakoff, A.A. The X-ray structure of a growth hormone-prolactin receptor complex. *Nature* **372**, 478–481 (1994).
19. Livnah, O. *et al.* Functional mimicry of a protein hormone by a peptide agonist: the EPO receptor complex at 2.8 Å. *Science* **273**, 464–471 (1996).
20. Syed, R.S. *et al.* Efficiency of signalling through cytokine receptors depends critically on receptor orientation. *Nature* **395**, 511–516 (1998).
21. Grotzinger, J., Kernebeck, T., Kallen, K.J. & Rose-John, S. IL-6 type cytokine receptor complexes: hexamer, tetramer or both? *Biol. Chem.* **380**, 803–813 (1999).
22. Takagi, J., Petre, B.M., Walz, T. & Springer, T.A. Global conformational rearrangements in integrin extracellular domains in outside-in and inside-out signaling. *Cell* **110**, 599–611 (2002).
23. Pflanz, S., Kurth, I., Grotzinger, J., Heinrich, P.C. & Muller-Newen, G. Two different epitopes of the signal transducer gp130 sequentially cooperate on IL-6-induced receptor activation. *J. Immunol.* **165**, 7042–7049 (2000).
24. Ohi, M., Li, Y., Cheng, Y. & Walz, T. Negative staining and image classification—powerful tools in modern electron microscopy. *Biol. Proced. Online* **6**, 23–34 (2004).
25. Frank, J. *et al.* SPIDER and WEB: processing and visualization of images in 3D electron microscopy and related fields. *J. Struct. Biol.* **116**, 190–199 (1996).
26. Radermacher, M., Wagenknecht, T., Verschoor, A. & Frank, J. Three-dimensional reconstruction from a single-exposure, random conical tilt series applied to the 50S ribosomal subunit of *Escherichia coli*. *J. Microsc.* **146**, 113–136 (1987).
27. Stewart, A. & Grigorieff, N. Noise bias in the refinement of structures derived from single particles. *Ultramicroscopy* **102**, 67–84 (2004).
28. Rosenthal, P.B. & Henderson, R. Optimal determination of particle orientation, absolute hand, and contrast loss in single-particle electron cryomicroscopy. *J. Mol. Biol.* **333**, 721–745 (2003).
29. Jones, T.A., Zou, J.Y., Cowan, S.W. & Kjeldgaard, M. Improved methods for building protein models in electron density maps and the location of errors in these models. *Acta Crystallogr. A* **47**, 110–119 (1991).